Article

Amplification in Mechanical Properties of a Lead Rubber Bearing for Various Exposure Times to Low Temperature

Cansu Yasar [1,*], Volkan Karuk [1], Onur Kaplan [2], Esengul Cavdar [1] and Gokhan Ozdemir [1]

[1] ESQUAKE Seismic Isolator Test Laboratory, Eskisehir Technical University, Eskisehir 26555, Turkey
[2] College of Engineering and Technology, American University of the Middle East, Egaila 54200, Kuwait
* Correspondence: c.yasar@eskisehir.edu.tr

Abstract: In this paper, new formulations to predict the change in mechanical properties, namely, post-yield stiffness and characteristic strength of lead rubber bearings (LRBs) at low ambient temperatures, are proposed based on test results. Proposed formulations consider not only the effect of low temperature but also the effect of exposure time to low temperature. Accordingly, a full-scale LRB was tested dynamically after being conditioned at temperatures of -20, -10, 0, and 20 °C for 3, 6, and 24 h. During the displacement-controlled cyclic tests, various levels of shear strain were applied to the isolator with loading frequencies of 0.1 Hz and 0.5 Hz. Then, force-displacement curves of LRB were recorded, and the corresponding amplifications in its hysteretic properties were noted. The accuracy of existing equations to estimate the amount of amplification in mechanical properties was evaluated through the experimental results. It was found that the existing formulas do not represent the effect of exposure time on LRB characteristics at low temperatures. On the other hand, the proposed equations result in highly accurate estimations of post-yield stiffness and characteristic strength of LRB at low temperatures for different exposure times.

Keywords: lead rubber bearings; seismic isolator; low temperature; mechanical properties

1. Introduction

One of the most widely used seismic isolation systems worldwide is lead rubber bearings (LRBs). It consists of layers of rubber and steel plates bonded on top of each other, with a lead core placed in the center. In this system, rubber is responsible for low horizontal stiffness, while the lead core provides enhanced energy dissipation capacity. Steel plates increase the vertical stiffness of the isolator [1,2]. The horizontal stiffness and strength of the isolator are two basic parameters in the design of seismically isolated structures [3]. In the experimental studies that focused on the variation of these two parameters when the isolator was exposed to low ambient temperatures, test specimens were mostly comprised of rubber samples rather than the full-scale isolator [4–12]. The common result of these studies is that there is an increase in rubber stiffness, especially at temperatures below 0 °C. On the other hand, exposure time to low temperatures was not considered as a parameter in most of these studies. However, the impact of exposure time was studied by Yakut and Yura [5,6] with rubber bearings having dimensions of $229 \times 356 \times 44.5$ mm. In their research, the exposure times were chosen as 1, 2, 4, 5, and 8 days to low temperatures of -30, -20, and -10 °C. The authors performed cyclic loadings at 30% shear strain and 0.01 Hz loading frequency. They emphasized that the increase in stiffness of rubber bearings is considerably sensitive to the exposure time of low temperatures. Cardone and Gesualdi [10] conducted various tests with 35×35 mm rubber samples. The tests were repeated for exposure times of 1, 4, 8, and 24 h to temperatures ranging from -20 to 40 °C. In their experimental program, shear strains ranged from 25 to 125%, and the loading frequency was 0.5 Hz. Cardone and Gesualdi [10] stated that the stiffness of the rubber increased significantly at low temperatures. The authors also indicated that such

amplification might result in shear forces larger than the design forces in the bearing and the bridge piers.

The above-mentioned studies are performed either with small rubber specimens rather than large-size LRB or at small shear strains that are compatible with service loadings. In these studies, tested bearings are primarily used to cope with both expansion/contraction due to thermal effects and bridge traffic loads. Such bearings fail to provide any protection against earthquakes. In regions with high seismicity, LRBs have been used to decouple the structure from the adverse effects of ground motions. Thus, experimental data related to the low-temperature behavior of LRBs needs to be improved. The first study in the literature investigating the low-temperature behavior of LRBs was conducted by Robinson [13]. The author considered a 356 × 356 mm square LRB and tested the sample after being conditioned at temperatures of −15 and −35 °C. The displacement subjected to LRB during the cyclic motion corresponds to 50% shear strain. Similarly, Hasegawa et al. [14] performed dynamic tests with a 250 mm diameter LRB for a shear strain of 100%. The authors investigated the hysteretic properties of LRB under temperatures of −20, 0, 20, and 40 °C. Then, Constantinou et al. [15] tested a 381 mm diameter LRB with a lead core diameter of 70 mm. The amplitude of lateral sinusoidal motion corresponds to a shear strain of 58%, and tests were repeated for temperatures of 20 and −26 °C. Based on the test results, the authors proposed some modification factors to estimate the mechanical properties at low temperatures. In a similar way, Li et al. [16] obtained the property modification factors by testing LRBs at temperatures ranging from −40 to 40 °C. Another study that investigates the modification in mechanical properties of LRB was performed by Cho et al. [17]. Apart from the previous studies, the authors selected a large-size LRB with rubber and lead core diameters of 860 mm and 170 mm, respectively. LRB was tested dynamically at a shear strain of 82%. The temperatures chosen were −20, −10, 0, and 23 °C. Similarly, Park et al. [18] assessed the effect of low temperature using a large-size LRB with a diameter of 800 mm. The temperatures considered by Park et al. [18] range from −10 to 40 °C, and displacement-controlled tests were applied at 100% shear strain. The authors proposed equations to predict the amplification in mechanical properties of the tested LRB at low temperatures. Mendez-Galindo et al. [19] also carried out low-temperature tests with a 550 × 550 × 236 mm square LRB. The LRB was conditioned at temperatures of −8 and −30 °C for 72 h and tested at shear strains ranging from 25% to 125% for −8 °C and 25% to 75% for −30 °C. The authors underlined an increase in both characteristic strength and post-yield stiffness of the LRB. Yet another study regarding the mechanical properties of LRB at low temperatures was conducted by Zhang and Li [20]. The authors tested a 220 mm diameter LRB when exposed to temperatures of −30, −20, 0, and 20 °C. Finally, Cavdar et al. [21] performed experiments with an LRB having rubber and lead core diameters of 1020 mm and 190 mm, respectively. The LRB was subjected to sinusoidal motion with a shear strain of 100% after being conditioned at 20 and −30 °C. The common output of the studies cited above is that both post-yield stiffness and characteristic strength of the tested LRBs increase with decreasing temperature, and the amount of amplification in characteristic strength is found to be larger than that of post-yield stiffness.

The literature review showed that the number of studies investigating the low-temperature response of rubber bearings is quite large. However, in particular, experimental data on the response of large-size LRBs exposed to low temperatures are scarce and need to be improved. Moreover, the exposure time to low temperatures was not considered as a parameter in any of the previous studies performed with LRBs. In addition, the shear strain level applied to LRBs in previous studies is mostly less than 100%. The displacement values that seismic isolators may undergo during an earthquake may be greater than those corresponding to 100% shear strain. Thus, there is a need to conduct a systematic research program to evaluate the effect of low temperature and exposure time on the hysteretic properties of an LRB for shear strains greater than and equal to 100%. It is also essential to investigate whether the modification factors available in the literature to represent amplifications in mechanical properties of LRBs at various ambient temperatures

are valid or not under different loading protocols. For this purpose, an 850 mm diameter LRB was tested at temperatures of −20, −10, 0, and 20 °C for 3, 6, and 24 h exposure times. Experiments were conducted with a single LRB for two levels of shear strains (100 and 134%) and loading frequencies (0.1 Hz and 0.5 Hz). Then, the efficiency of existing modification factors to estimate variation in hysteretic properties is presented comparatively. Finally, new equations were proposed to predict the post-yield stiffness and characteristic strength of LRB at low temperatures also considering the effect of exposure time.

2. Experimental Program

2.1. Test Specimen

The LRB under investigation has a diameter of 850 mm with a lead core of 220 mm in diameter. It consists of 18 layers of rubber with 11 mm thickness each and 17 layers of steel with an individual layer thickness of 3 mm. The LRB's height is 339 mm, including the top and bottom plates and the end shim at the top. Figure 1 presents the geometric properties of the tested LRB. The shear modulus of the rubber at 100% shear strain is 0.6 MPa.
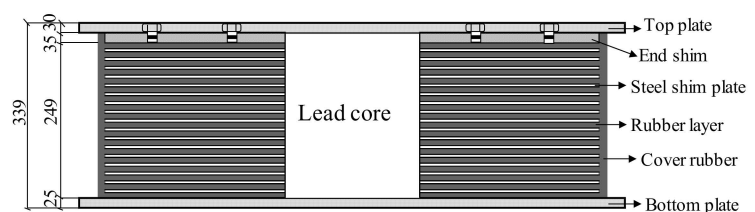

(a)   (b)

Figure 1. (**a**) View (**b**) geometry of the tested lead rubber bearing (units are in mm).

2.2. Test Setup

The LRB presented in Figure 1 was tested at the ESQUAKE Seismic Isolator Test Laboratory of Eskişehir Technical University. The test setup enables the application of force and displacement-controlled dynamic excitations to test specimens in both horizontal and vertical directions. Thus, the vertical force applied to the specimen can be kept constant during the motion in the horizontal direction. The maximum loading capacities are 2.000 kN and 20.000 kN in the horizontal and vertical directions, respectively. In the horizontal direction, the maximum displacement capacity is equal to ±600 mm (See Figure 2a for test setup). The environmental chamber of ESQUAKE shown in Figure 2b facilitates the exposure of the LRB to low temperatures. The thermal chamber and test setup are placed next to each other, as seen in Figure 2c. The dimensions of the thermal room are 3 × 3 × 3 m, and it provides a minimum and maximum temperature of −40 and +50 °C, respectively.

2.3. Test Program and Methodology

The test protocol shown in Table 1 consists of displacement-controlled cyclic tests performed after the LRB was conditioned at ambient temperatures of −20, −10, 0, and 20 °C for 3, 6, and 24 h exposure times. The maximum lateral displacement applied during the cyclic motion is 266 mm, corresponding to 134% shear strain. This upper limit was decided based on the information provided by the manufacturer as the maximum design displacement of the LRB. In order to investigate the effect of isolator displacement on the behavior of the tested LRB, a shear strain of 100% was also included in the test program. The corresponding motion amplitude considered in the test is 198 mm for 100% shear strain. Another parameter that is the current research study's aim is loading frequency. For this purpose, loadings were repeated for different loading frequencies of 0.1 and 0.5 Hz.

(a)

(b)

(c)
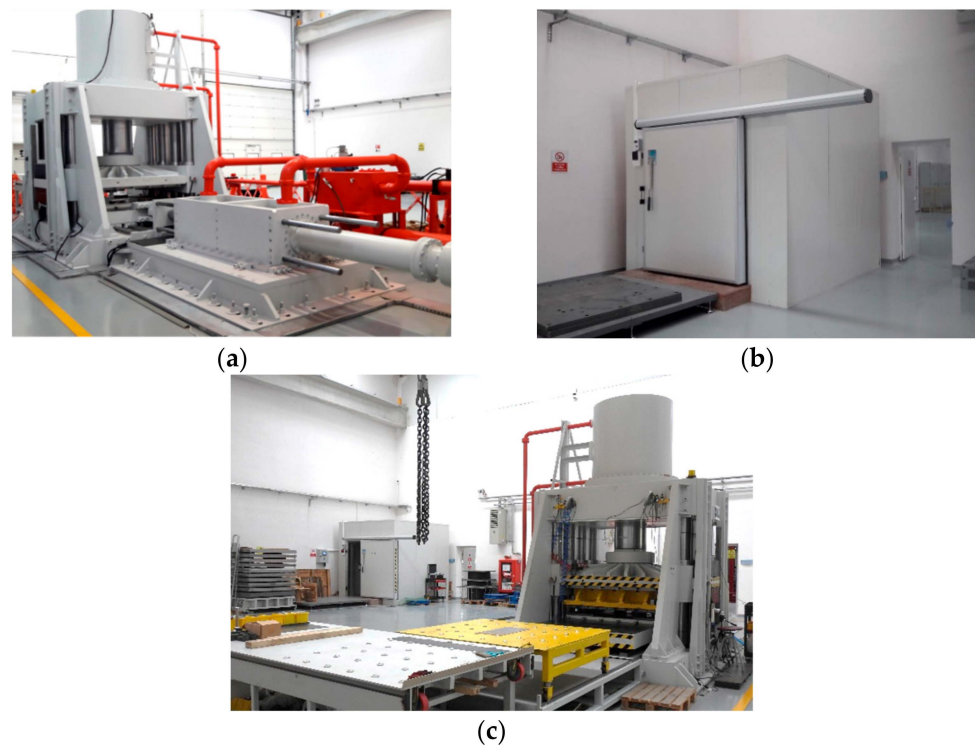
Figure 2. (**a**) Seismic isolator test device (**b**) environmental chamber (**c**) layout of the environmental chamber and test device.

Table 1. Loading protocol followed in the experimental program.

Test No	Temperature	Exposure Time (h)	Shear Strain (%)	Frequency (Hz)	Cycle Number
1	20 °C	-	100, 134	0.1, 0.5	3
2	0 °C	3, 6, 24	100, 134	0.1, 0.5	3
3	−10 °C	3, 6, 24	100, 134	0.1, 0.5	3
4	−20 °C	3, 6, 24	100, 134	0.1, 0.5	3

During the tests, three cycles of sinusoidal motion were applied to the LRB, as shown in Figure 3a,b for loading frequencies of 0.1 and 0.5 Hz, respectively. The vertical force acting on the LRB during the cyclic motion was 3177 kN, corresponding to a normal stress of 5.8 MPa.

(a)

(b)

$\gamma=\%134$
$\gamma=\%100$
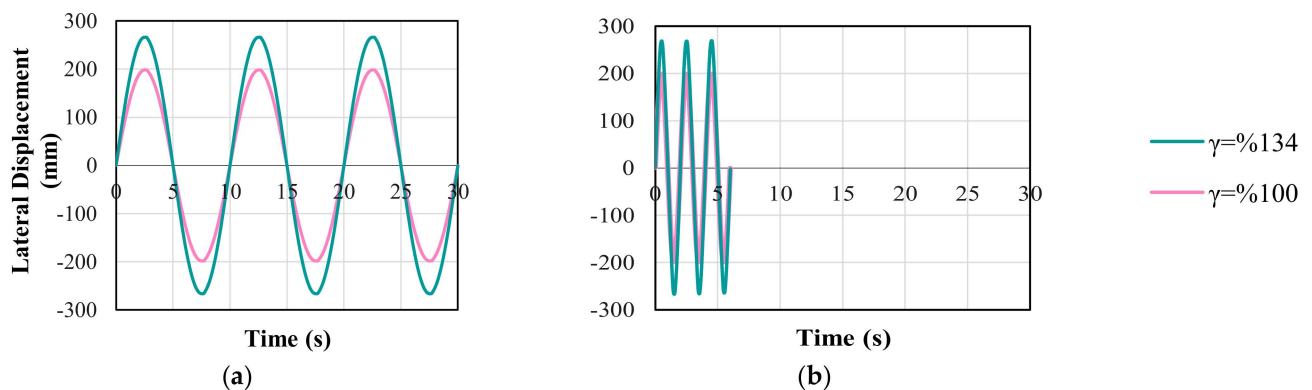
Figure 3. Applied loading history to lead rubber bearing for a frequency of (**a**) 0.1 Hz and (**b**) 0.5 Hz.

The test campaign started with the reference test (20 °C) defined in Table 1. Then, the low-temperature tests were conducted. The low ambient temperatures included in the test protocol were provided by the thermal chamber shown in Figure 2b. First, the LRB under investigation was conditioned in the thermal chamber at the desired temperature and exposure time. Afterward, it was removed from the thermal chamber and connected to the test device, and tested under three cycles of motion in accordance with code specifications [22] at laboratory conditions (see Figure 4). This process was repeated for each and every loading case given in Table 1. The time between the removal of LRB from the thermal chamber and the end of the cyclic motion was less than 10 min. It is to be noted that there was a 24-h dwell period between each loading case so that the LRB would warm up to its initial value. Thus, the change in the characteristics of the LRB due to the previous loading was reverted prior to the new loading process.


(**a**)   (**b**)

Figure 4. For −20 °C, 24 h exposure time loading combination (**a**) LRB placed in the seismic isolator test device (**b**) a view from cyclic motion.

3. Experimental Results

During the tests, force-displacement curves of the full-size LRB were recorded for each loading combination given in Table 1. In this section, recorded hysteretic curves will be presented comparatively. However, first, in order to ensure that there is no permanent deformation on the LRB after all the loading sequences, pictures of the LRB both before the initial loading and after the final loading cases are given in Figure 5. In addition, as shown in Figure 6, having almost identical reference force-displacement curves reveals that the cyclic response of the LRB remains almost the same after the testing campaign is completed. Thus, testing the same LRB at all loading cases defined in Table 1 did not introduce any bias.


(**a**)   (**b**)
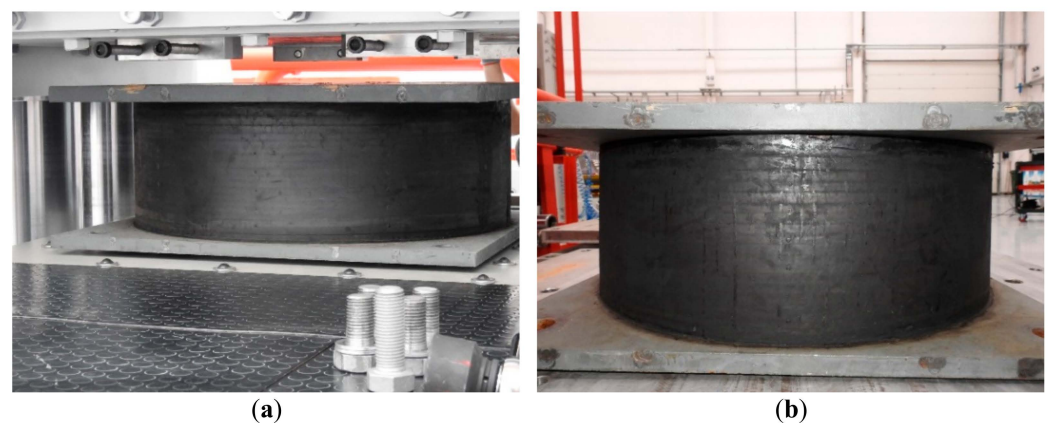
Figure 5. Physical condition of the LRB (**a**) before the initial loading and (**b**) after the final loading cases.
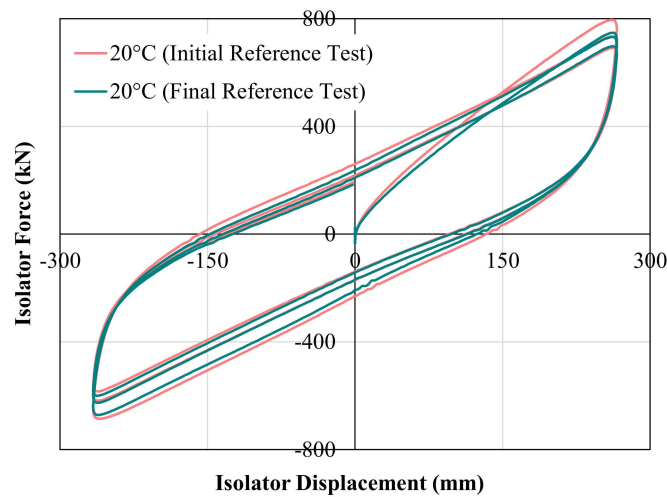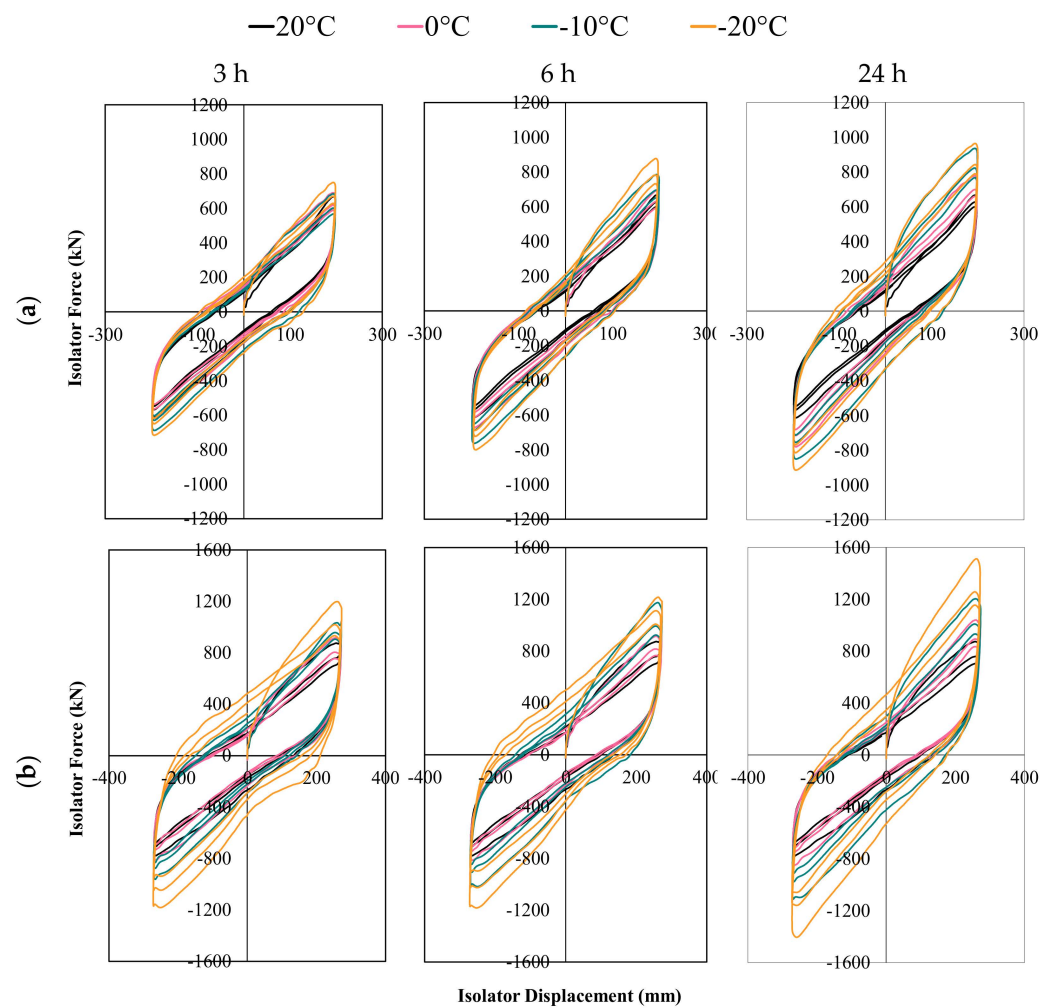
Figure 6. Comparison of reference force-displacement curves of the LRB.

Figures 7 and 8 depict force-displacement curves recorded under different loading combinations defined as functions of shear strain, ambient temperature, and exposure time to low temperature. It is clear that both the strength and lateral stiffness of the LRB tend to increase regardless of the loading frequency when the ambient temperature decreases. Another observation is that the hysteretic behavior of the LRB is sensitive to exposure time at low temperatures.
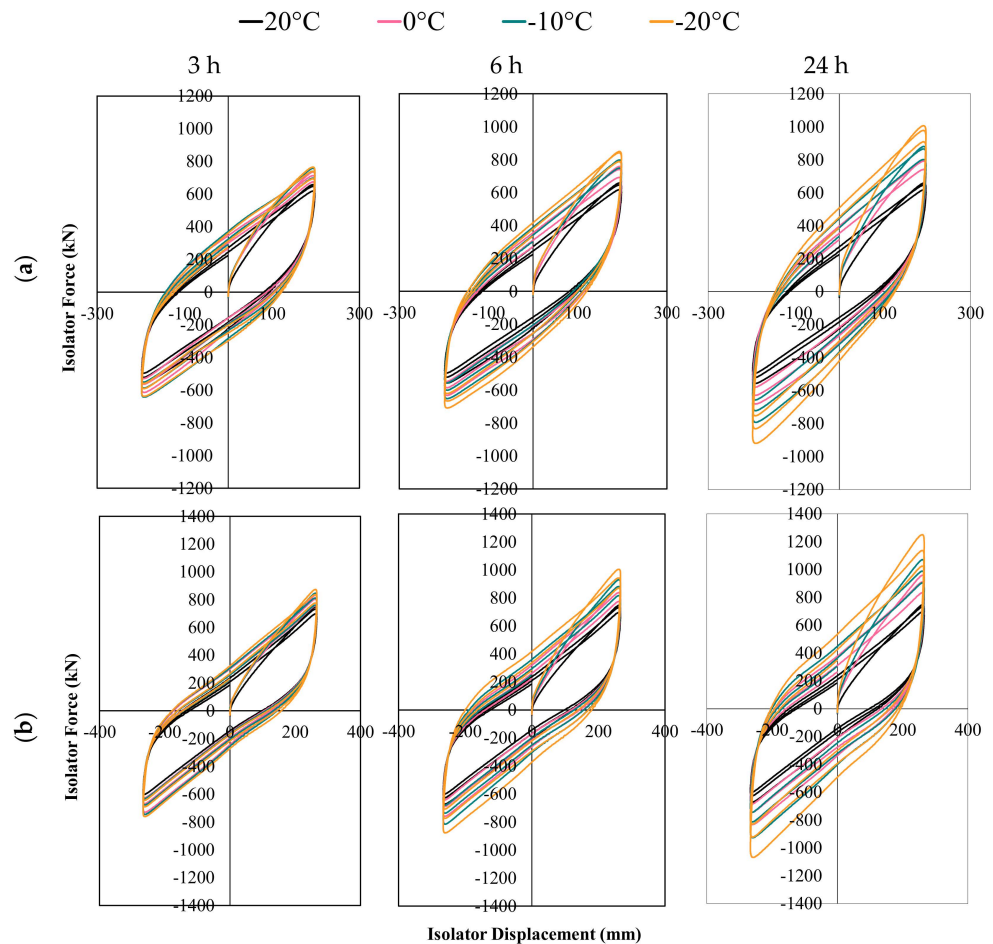
Figure 7. Comparison of force-displacement curves obtained for different shear strains, temperatures, and exposure times at a loading frequency of 0.1 Hz for (**a**) 100% and (**b**) 134% shear strains.

Figure 8. Comparison of force-displacement curves obtained for different shear strains, temperatures, and exposure times at a loading frequency of 0.5 Hz for (**a**) 100% and (**b**) 134% shear strains.

In order to reveal the trend of change in isolator mechanical properties better, characteristic strength, Q, and post-elastic stiffness, k_2 (see Figure 9a for definitions) of the LRB were obtained using recorded force-displacement curves. Q and k_2 are calculated by the straight-line fit method suggested by EN-15129 [22]. In this study, the Least Square Method (LSM) is used to find the best fit for data by minimizing the sum of the squared errors. In Figure 9b, the application of LSM is described for a representative force-displacement curve. Accordingly, (Q_{pos} and Q_{neg}) and ($k_{2(upper)}$ and $k_{2(lower)}$) values are acquired for each cycle of the motion as defined in Figure 9b. Then, the ultimate Q and k_2 values are computed by Equations (1) and (2), respectively. Tables 2 and 3 present the corresponding isolator characteristics calculated for different loading cases.

$$Q = \frac{Q_{pos} - Q_{neg}}{2} \tag{1}$$

$$k_2 = \frac{k_{2(upper)} + k_{2(lower)}}{2} \tag{2}$$

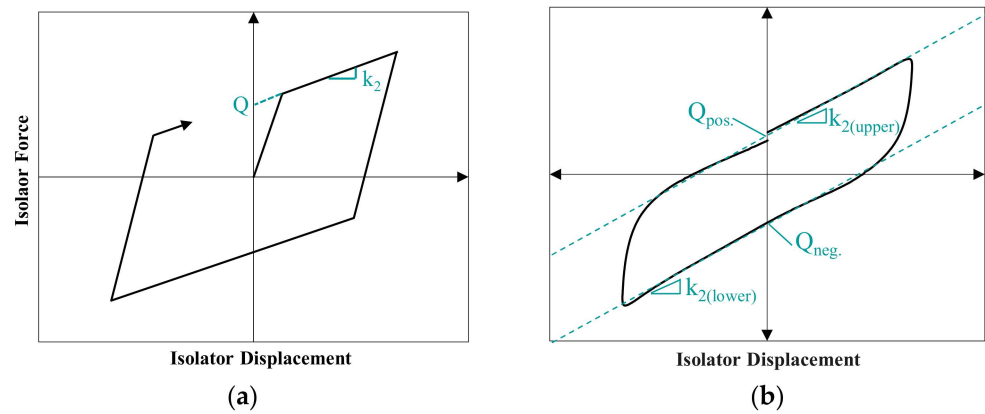**Figure 9.** (**a**) Idealized bilinear force-displacement relation of LRB (**b**) application of LSM method.

Table 2. Mechanical properties of LRB computed at the frequency of 0.1 Hz.

	Temperature (°C)	−20			−10			0			20
	Exposure Time (h)	3	6	24	3	6	24	3	6	24	-
100% Shear Strain	$k_{2\,(1st\ cycle)}$, kN/m	2286	2564	3054	2288	2442	2748	2234	2312	2518	2224
	$k_{2\,(2nd\ cycle)}$, kN/m	2196	2525	2919	2177	2368	2626	2127	2236	2398	2104
	$k_{2\,(3rd\ cycle)}$, kN/m	2124	2404	2752	2101	2262	2476	2046	2143	2284	2017
	$Q_{(1st\ cycle)}$, kN	296	344	433	298	310	373	269	291	321	222
	$Q_{(2nd\ cycle)}$, kN	253	305	373	255	267	319	232	250	280	196
	$Q_{(3rd\ cycle)}$, kN	224	268	318	224	230	272	206	219	244	178
134% Shear Strain	$k_{2\,(1st\ cycle)}$, kN/m	1941	2080	2450	1914	1987	2168	1908	1934	2031	1822
	$k_{2\,(2nd\ cycle)}$, kN/m	1848	1984	2270	1829	1916	2062	1815	1848	1936	1745
	$k_{2\,(3rd\ cycle)}$, kN/m	1781	1904	2158	1768	1841	1973	1757	1784	1858	1697
	$Q_{(1st\ cycle)}$, kN	297	385	493	282	331	413	272	294	352	226
	$Q_{(2nd\ cycle)}$, kN	244	306	391	234	272	330	229	240	285	194
	$Q_{(3rd\ cycle)}$, kN	209	254	320	204	231	276	201	206	240	175

Table 3. Mechanical properties of LRB computed at the frequency of 0.5 Hz.

|	Temperature (°C)	−20			−10			0			20
	Exposure Time (h)	3	6	24	3	6	24	3	6	24	-
100% Shear Strain	$k_{2\,(1st\ cycle)}$, kN/m	2431	2928	3122	2303	2694	3106	2254	2373	2695	2000
	$k_{2\,(2nd\ cycle)}$, kN/m	2251	2687	2866	2155	2452	2792	2113	2221	2496	1865
	$k_{2\,(3rd\ cycle)}$, kN/m	2158	2568	2721	2070	2331	2652	2033	2122	2382	1808
	$Q_{(1st\ cycle)}$, kN	223	241	307	198	223	277	183	191	215	156
	$Q_{(2nd\ cycle)}$, kN	185	194	253	166	181	212	156	162	177	131
	$Q_{(3rd\ cycle)}$, kN	170	174	230	153	165	188	143	147	158	122
134% Shear Strain	$k_{2\,(1st\ cycle)}$, kN/m	2529	2700	3271	2456	2620	2693	2153	2163	2214	2113
	$k_{2\,(2nd\ cycle)}$, kN/m	2415	2506	2892	2319	2337	2388	1965	1990	2017	1914
	$k_{2\,(3rd\ cycle)}$, kN/m	2275	2333	2707	2227	2197	2230	1897	1915	1943	1829
	$Q_{(1st\ cycle)}$, kN	477	472	490	315	350	368	243	239	256	237
	$Q_{(2nd\ cycle)}$, kN	389	393	373	260	277	284	191	193	206	190
	$Q_{(3rd\ cycle)}$, kN	330	333	322	237	246	253	171	178	188	172

In Tables 2 and 3, the results obtained for 20 °C are considered reference values. In order to have clear observations in terms of amplification in mechanical properties of the tested

LRB at low temperatures (-20 °C, -10 °C, and 0 °C), experimental data were normalized with the ones obtained from the reference tests. Accordingly, Figures 10 and 11 illustrate the normalized characteristic strength $Q/Q_{(20 °C)}$ at ambient temperatures of -20, -10, and 0 °C for 0.1 and 0.5 Hz loading frequencies, respectively. Figures 10 and 11 clearly show that the characteristic strength, Q, of the LRB increases with decreasing temperature. The amount of increase becomes more pronounced with longer exposure times at all temperatures. It is apparent that the time of exposure to low temperatures has a significant impact on the amplification of the LRB strength.
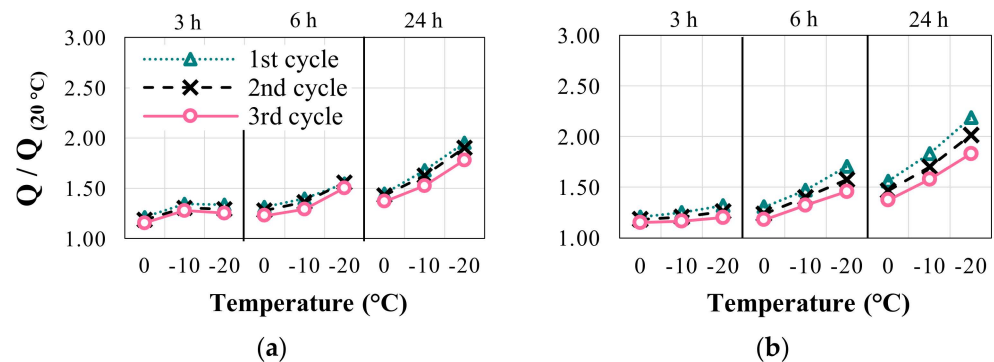

Figure 10. Comparison of normalized characteristic strengths for 0.1 Hz loading frequency at (**a**) 100% and (**b**) 134% shear strains.
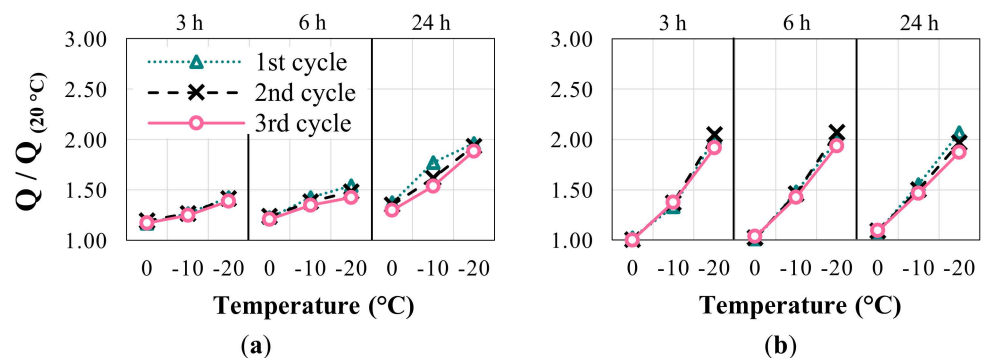
Figure 11. Comparison of normalized characteristic strengths for 0.5 Hz loading frequency at (**a**) 100% and (**b**) 134% shear strains.

In Figure 10, it is also observed that the amplification in LRB strength tends to decrease with the increasing number of loading cycles. Such observation can be ascribed to the temperature rises at the lead core of LRB during cyclic motion. Kalpakidis et al. [23] revealed that the strength of an LRB deteriorates during cyclic motion as a function of the lead core heating. The temperature rise at the lead core will result in a thermal transient, and the corresponding temperature of the lead core at each loading cycle will increase gradually. For instance, for the loading case where the temperature is -20 °C and exposure time is 24 h, the lead core temperature will be close to -20 °C at the 1st cycle. However, because of the temperature rise at the lead core, it will be greater than -20 °C in the 2nd and 3rd cycles. Accordingly, the amplifications in the strength of LRB with respect to the reference case will decrease with the increasing number of cycles. Apart from Figure 10, in Figure 11, the change in $Q/Q_{(20 °C)}$ ratios from cycle-to-cycle are very limited, especially for 134% shear strain. For data presented in Figure 11, the loading velocity is five times larger than the one in Figure 10. In the 0.5 Hz loading frequency case, the maximum loading velocities were 622 and 835 mm/s for 100 and 134% shear strains, respectively. In addition, the temperature rise in the lead core will be much higher compared to loading cases having 0.1 Hz frequency. As a result, the gradual deterioration in the strength of LRB will be higher at each cycle and has a very close trend with the deterioration in the reference test (see

Figure 12). Thus, the corresponding amplifications in the strength of LRB (or $Q/Q_{(20\,°C)}$ ratios) at each loading cycle attain almost identical values, as presented in Figure 11.
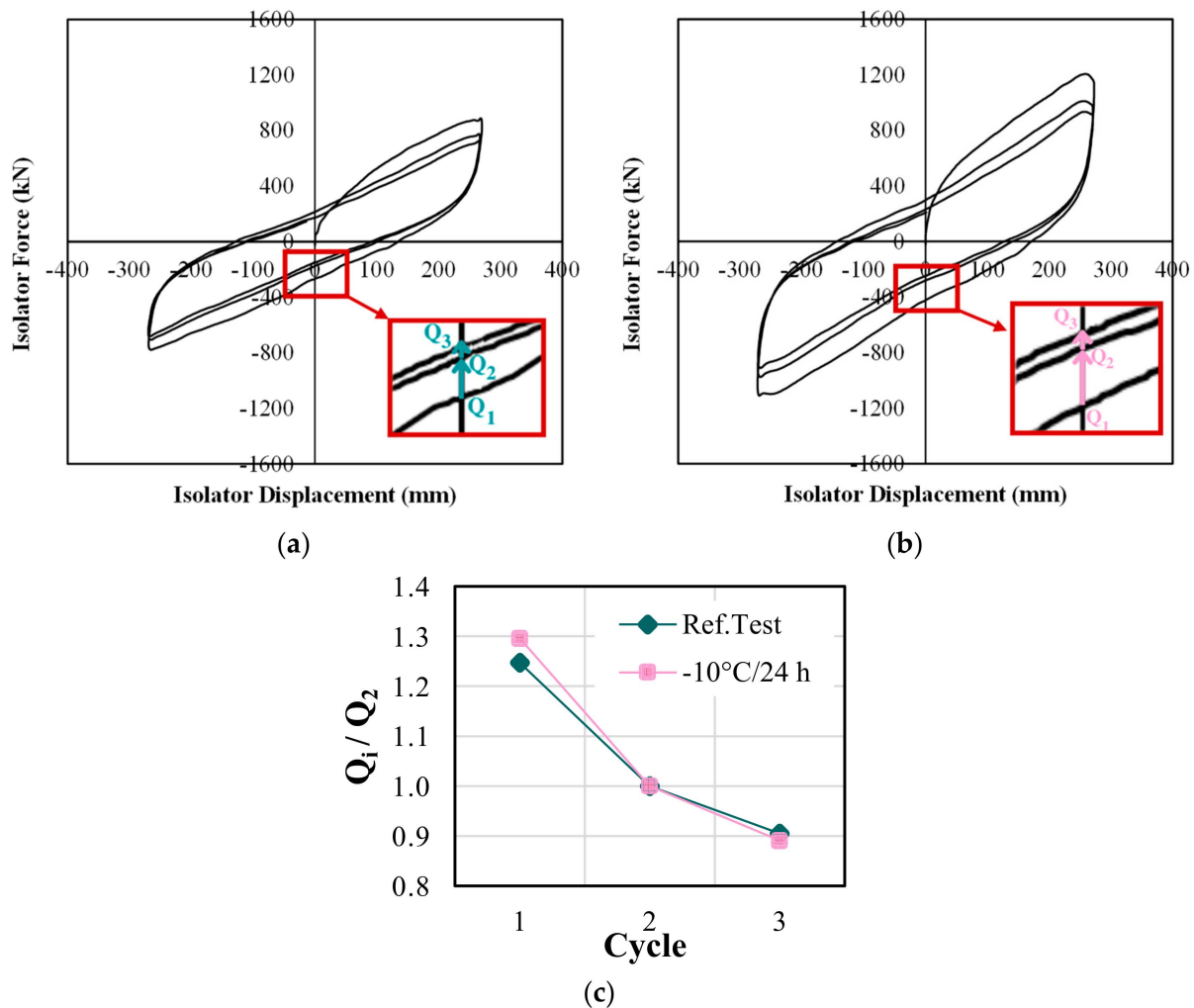

Figure 12. Force-displacement curves of the LRB for 134% shear strain and 0.5 Hz loading frequency (**a**) reference test (**b**) 24 h exposure time at −10 °C, (**c**) ratio of characteristic strength each cycle to that of the second cycle.

Figures 13 and 14 show the amplifications in post-yield stiffness of the LRB for different temperatures and exposure times. Post-yield stiffnesses computed for each temperature and exposure time are normalized with the ones calculated for 20 °C, $k_2/k_{2(20\,°C)}$. Similarly, Figures 13 and 14 indicate that $k_2/k_{2(20\,°C)}$ ratios increase with decreasing temperature and increasing exposure time. However, the amplifications in post-yield stiffness are less than those computed for characteristic strength. Furthermore, $k_2/k_{2(20\,°C)}$ ratios are almost not sensitive to changes in lead core temperature during the cyclic motion and remain the same at all cycles. It is because the thermal conductivity of rubber (0.16 W/mK) is very low compared to lead (35.3 W/mK). Hence, the temperature rise in the lead core does not change the temperature of the rubber layers during the test. Such observation is also parallel to the findings of Kalpakidis et al. [23]. It is also noted that amplifications in post-yield stiffness due to low-temperature exposure are higher for loadings with 0.5 Hz frequency compared to those with 0.1 Hz frequency.
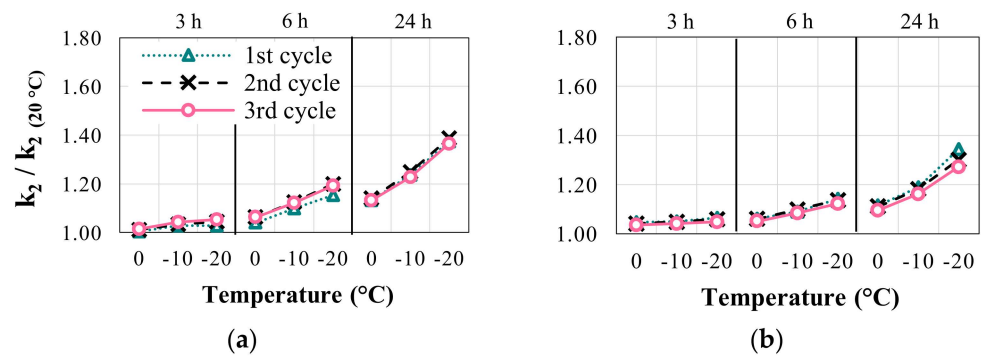
Figure 13. Comparison of normalized post-yield stiffness for 0.1 Hz loading frequency at (**a**) 100% and (**b**) 134% shear strains.
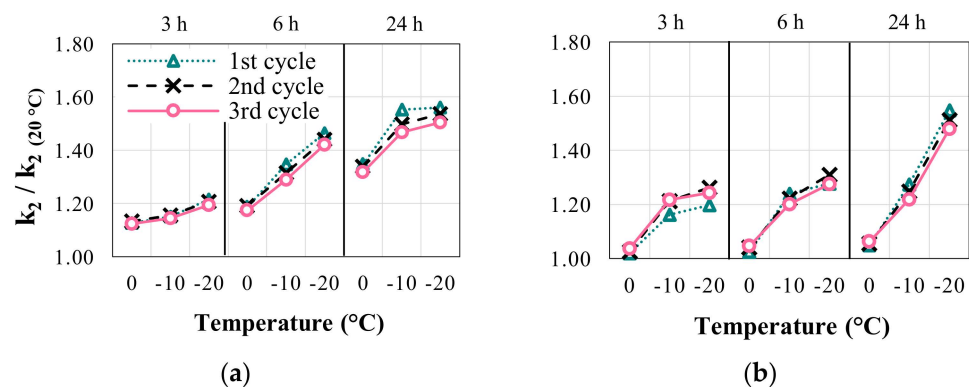
Figure 14. Comparison of normalized post-yield stiffness for 0.5 Hz loading frequency at (**a**) 100% and (**b**) 134% shear strains.

4. Accuracy of the Existing Formulations to Estimate the Amplifications in Isolator Characteristics

In the literature, there are studies that proposed modification factors to estimate the variation in mechanical properties of LRBs exposed to low temperatures. In this section, three of those studies (see Table 4) are cited to evaluate their accuracy in estimating the amplifications in both characteristic strength and post-yield stiffness. The reason for considering the proposals of Constantinou et al. [15], Li et al. [16], and Park et al. [18] is that they were conducted with large-size LRBs having similar dimensions to the LRB tested in this research study. Table 4 presents the amplification factors suggested for both characteristic strength and post-yield stiffness. Figures 15–18 are depicted to compare the experimentally calculated amplifications of the current study with the proposals of the studies cited above. Figures 15 and 16 present the comparisons for characteristic strength, Q, for loading frequencies of 0.1 and 0.5 Hz, respectively. In these figures, for 100% shear strain, it is clear that regardless of the loading frequency, the proposals given in Table 4 are consistent with the test results for all of the considered temperatures when the exposure time is 3 and 6 h. However, for an exposure time of 24 h, proposed amplification factors underestimate the computed ones, and the degree of underestimation increases with decreasing temperature. When the shear strain is 134%, the loading frequency seems to affect the accuracy of the proposed factors. For 0.1 Hz frequency, they provide close estimations for 3 and 6 h of exposure times. However, their estimations do not represent actual behavior when the exposure time is 24 h for all of the considered temperatures. For 0.5 Hz frequency, cited proposals lead to close or overestimated amplifications for −10 and 0 °C while they underestimate the amplification in Q for all of the exposure times at −20 °C. Figures 15 and 16 revealed that the existing proposals for estimation of the amplification in characteristic strength of LRB need to be improved to consider the effects of both exposure time and loading frequency.

Table 4. Amplification factors suggested for different temperatures.

|	Parameters	Temperature		
		0 °C	**−10 °C**	**−20 °C**
Constantinou et al. [15]	Q	1.20	1.40	–
	k_2	1.10	1.10	–
Li et al. [16]	Q	1.22	1.32	1.45
	k_2	1.04	1.10	1.14
Park et al. [18]	Q	1.19	1.30	1.42
	k_2	1.06	1.08	1.11

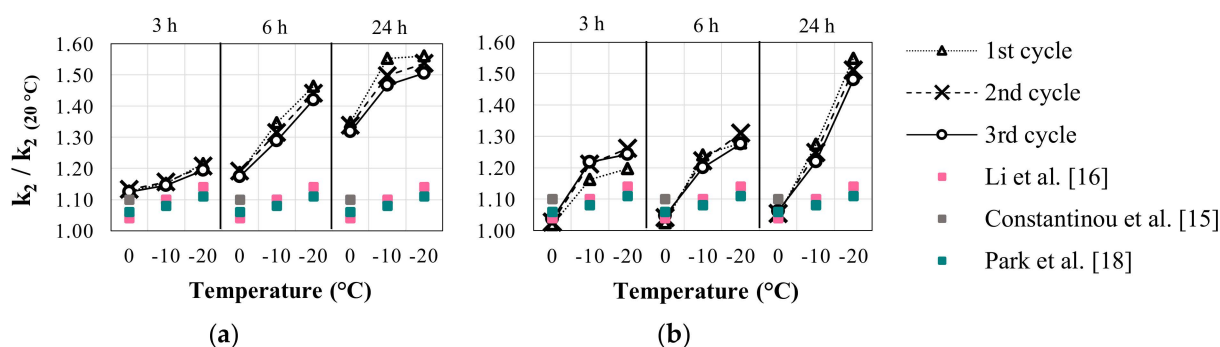"–" means there is no available amplification factor.
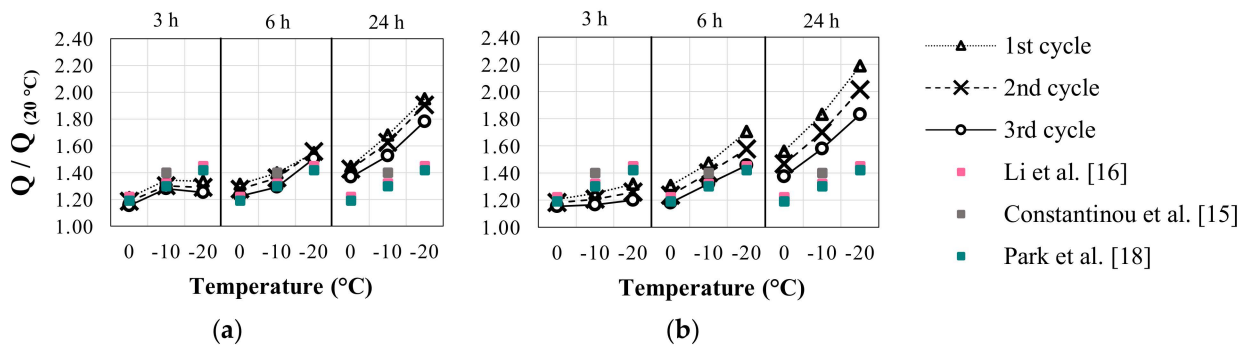
Figure 15. Comparison of amplifications in Q with the available amplification factors in the literature for 0.1 Hz loading frequency at (**a**) 100% and (**b**) 134% shear strains.
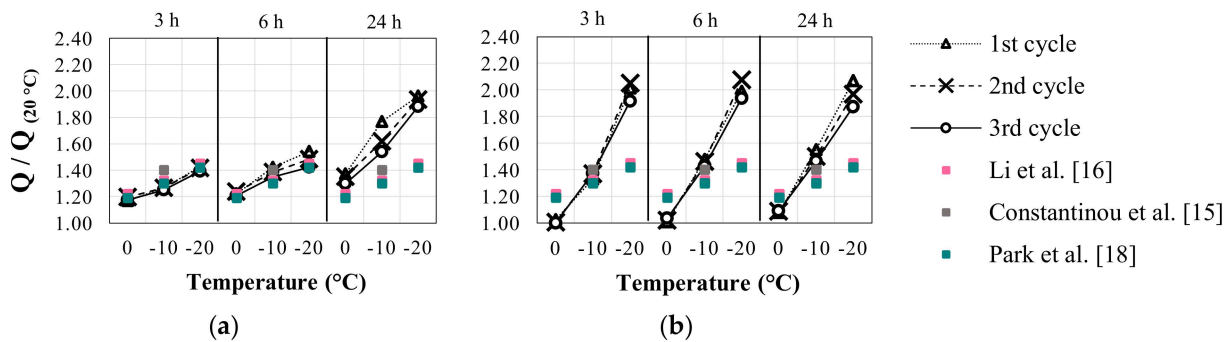
Figure 16. Comparison of amplifications in Q with the available amplification factors in the literature for 0.5 Hz loading frequency at (**a**) 100% and (**b**) 134% shear strains.
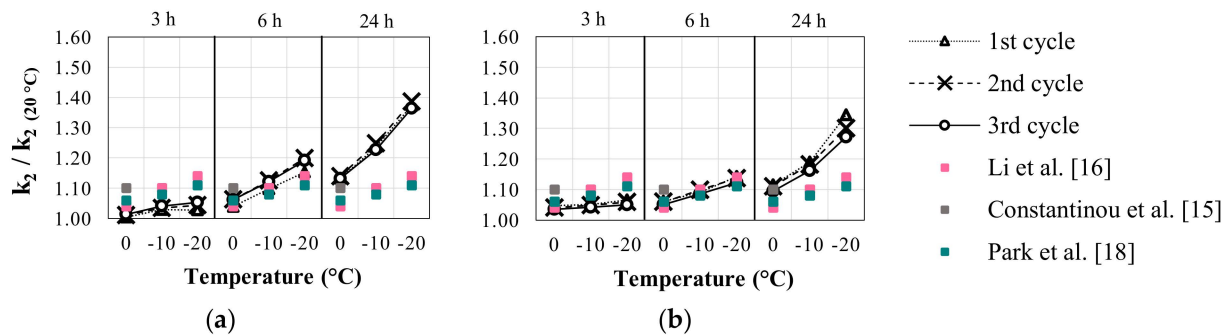
Figure 17. Comparison of amplifications in k_2 with the estimations of amplification factors in the literature for 0.1 Hz loading frequency at (**a**) 100% and (**b**) 134% shear strains.

Figure 18. Comparison of amplifications in k_2 with the estimations of amplification factors in the literature for 0.5 Hz loading frequency at (**a**) 100% and (**b**) 134% shear strains.

Figures 17 and 18 compare the estimations of amplification factors given in Table 4 with experimental data in terms of post-yield stiffness, k_2. Figure 17 presents very similar results to the ones for characteristic strength. Amplification factors of Table 4 give very close estimations for all temperatures when the exposure time is 3 and 6 h. On the other hand, they underestimate experimental data for 24 h exposure time. In Figure 18, where the loading frequency is 0.5 Hz, the amplifications in post-yield stiffness are underestimated for almost all of the temperatures and exposure times. Furthermore, the amount of underestimation tends to increase with decreasing temperature and increasing exposure time. Such observations clearly indicate that the cited proposals used to estimate amplification in post-yield stiffness of LRBs also do not cover the effects of exposure time and loading frequency.

5. Proposed Formulations to Consider Also the Effects of Exposure Time and Loading Frequency

This section proposes empirical relations to predict the amplifications in both characteristic strength and post-yield stiffness of LRBs due to low-temperature exposure. The proposed formulations were obtained from regression analyses performed using the genetic programming (GP) methodology. Genetic Programming (GP) is an extension of Genetic Algorithms (GAs), an optimization technique based on the Darwinian concept of survival of the fittest. GP was invented by Cramer in 1985 [24] and further developed by Koza [25]. The purpose of GP is to obtain an alternative to fixed-length solutions by developing different nonlinear structures in terms of sizes and shapes. The main difference between GAs and GP arises from the definition of entities. In GAs, entities are defined by fixed-length linear sequences (chromosomes). On the other hand, they are represented by nonlinear forms with distinct sizes and shapes (parse trees). Gene Expression Programming (GEP) software, which is used in this study, is a combination of GAs and GP [26]. In the most general sense, Gene Expression Programming (GEP) is used in experimental studies for optimization, development of mathematical models based on input-output data, and classification. Especially in civil engineering problems, GEP has been used to develop formulations based on experimental and analytical studies instead of traditional regression and neural network modeling techniques [27–31].

In this study, GeneXproTools [32] program is used to generate the GEP-based regression model for experimental data. This model was applied to estimate the $Q/Q_{(20\,°C)}$ and $k_2/k_{2(20\,°C)}$ ratios of LRBs exposed to low temperatures. For this purpose, first, the dependent and independent variables were introduced to the software. The loading parameters based on the experiments, namely temperature (T), exposure time (t), and amplitude (A), represent the independent variables. The amount of amplification corresponding to each loading combination (see Figures 10, 11, 13 and 14) constitutes the dependent values. After this phase, there are five major steps in preparing to use GEP:

i.   *Selection of the fitness function*: Fitness is a measure that can evaluate the proposed model's performance. For this problem, the fitness was measured by Equation (3)

where R is the selection range, $P_{(ij)}$ is the estimation of the individual program i for fitness case j, and T_j is the target value for fitness case j. The maximum fitness value, $f_{max} = 1000$, uses an absolute error of 100 as the selection range, and error precision equals 0.01 with 10 fitness cases [26].

$$f_i = \sum_{j=1}^{n} \left(R - \left| P_{(ij)} - T_j \right| \right) \tag{3}$$

ii. *Selection of the set of function*: For this problem, exponential and four arithmetic operator function sets are chosen, thus giving F = {+, −, *, /, Exp}.

iii. *Selection of the chromosomal architecture*: GEP is composed of genes having two domains called the head and tail. The head domain is employed to codify the functions selected to represent the problem. On the other hand, the tail domain acts as a buffer to ensure the formation of only valid structures. For the selected problem, the length of the head (h) needs to be defined. In addition, the length of the tail (t) is a function of h. Three genes per chromosome and h = 7 were used in this study.

iv. *Selection of the linking function*: GEP consists of two main parameters: chromosomes and expression trees (ETs). ETs are the representations of the genetic information codified in the chromosomes. The ETs can be composed of only one subunit or multi-subunit. Subunits are linked together by the linking function, which can be defined as addition, subtraction, multiplication, and division. In this study, we linked the sub-ETs via addition [26].

v. *Selection of the set of genetic operators*: GEP takes an initial population and then evolves this population using one or more genetic operators. A combination of all modification operators, namely mutation, inversion, three types of transposition, and three types of recombination, was used in this study [26].

Empirical expressions derived were obtained separately for 0.1 and 0.5 Hz loading frequencies and given in Tables 5 and 6. The fitness values at which each regression analysis was terminated are given in Table 7. The accuracy of the proposed formulations to estimate the amplifications in characteristic strength and post-yield stiffness of the tested LRB is discussed by means of Figures 19–22. Accordingly, computed estimations using formulations of Tables 5 and 6 are found to be in good agreement with the experimental data obtained from LRB tests under different temperatures and exposure times. It can be said that the proposed formulations are sufficiently successful in predicting the mechanical properties of the tested LRB under different low ambient temperatures and exposure times.

Table 5. The proposed empirical expressions for LRB's characteristic strength at low ambient temperatures.

Loading Frequency	Characteristic Strength
0.1 Hz	$\dfrac{Q}{Q_{(20\,°C)}} = \exp\left(3.5 \times 10^{-4}A\right) + \dfrac{(t - 0.8)\,(13.7 - T)}{t^2 + 351}$
0.5 Hz	$\dfrac{Q}{Q_{(20\,°C)}} = \exp\left(\dfrac{\frac{A}{t} - AT}{8867}\right) + \dfrac{t}{A - 130}$

Table 6. The proposed empirical expressions for LRB's post-yield stiffness at low ambient temperatures.

Loading Frequency	Post-Yield Stiffness
0.1 Hz	$\dfrac{k_2}{k_{2(20\,°C)}} = \dfrac{2t^2 + T}{(t)\,(6.4T + A + 3t - 8.9)} + \exp\left(\dfrac{T + 0.5t - 1.5}{4.9T - A + 1.6}\right)$
0.5 Hz	$\dfrac{k_2}{k_{2(20\,°C)}} = \dfrac{53t - 5.3Tt}{At + 5.5A} + \exp\left(\dfrac{t}{(T - 6.7)(A - 2T - 9.9t + 4.6)}\right)$

**Table 7.** Best fitness values of the regression analyses.

| Loading Frequency	Mechanical Property	Best Fitness
0.1 Hz	Q	930
0.1 Hz	k_2	979
0.5 Hz	Q	906
0.5 Hz	k_2	957

(a)　　　　　　　　　　　　　(b)
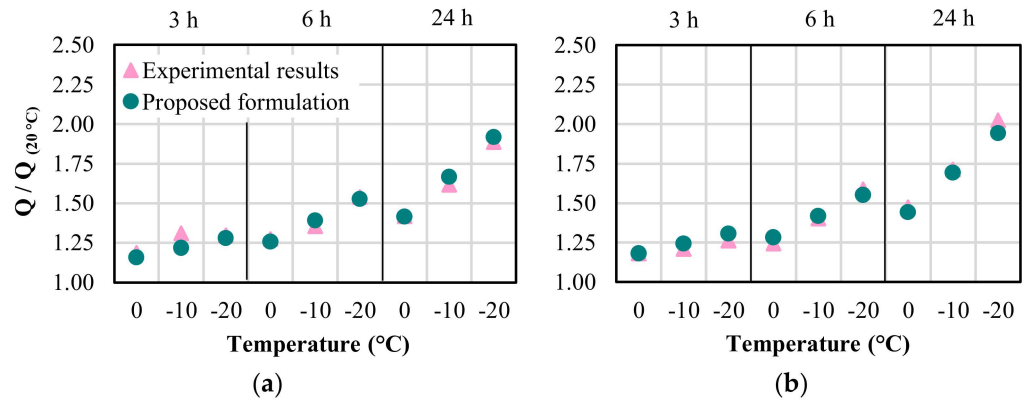
Figure 19. Comparison of experimental amplifications in Q with the proposed formulation estimations for 0.1 Hz loading frequency at (**a**) 100% and (**b**) 134% shear strains.

(a)　　　　　　　　　　　　　(b)
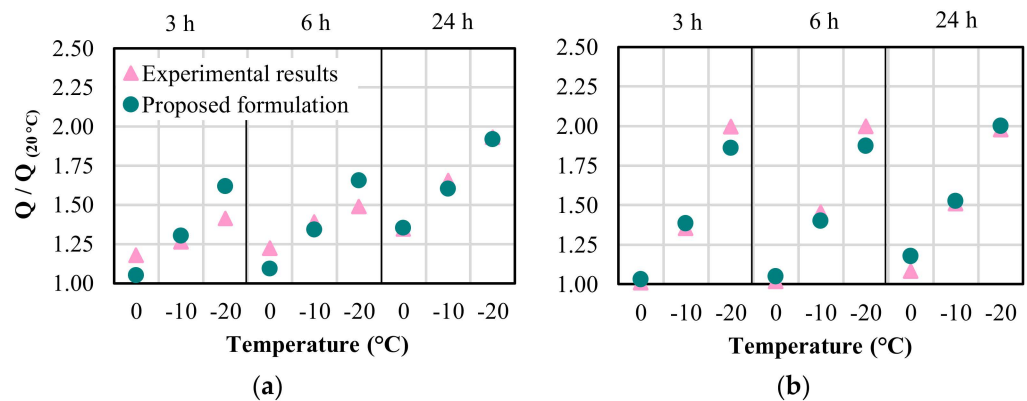
Figure 20. Comparison of experimental amplifications in Q with the proposed formulation estimations for 0.5 Hz loading frequency at (**a**) 100% and (**b**) 134% shear strains.

(a)　　　　　　　　　　　　　(b)
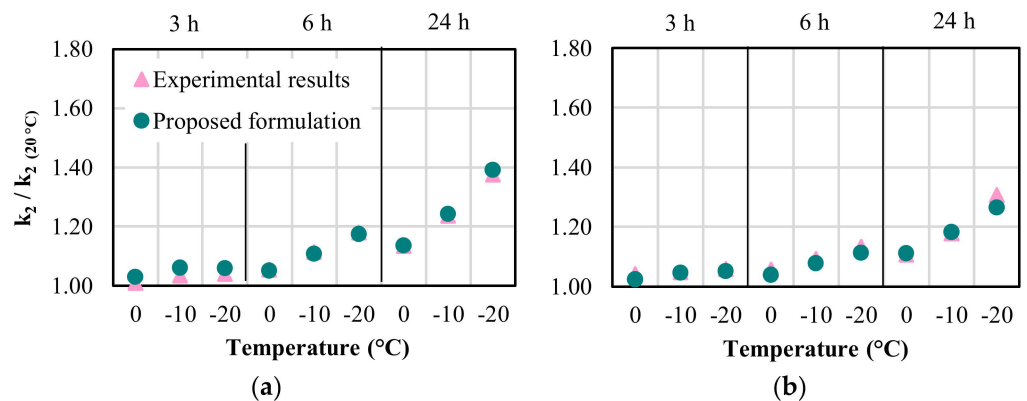
Figure 21. Comparison of experimental amplifications in k_2 with the proposed formulation estimations for 0.1 Hz loading frequency at (**a**) 100% and (**b**) 134% shear strains.
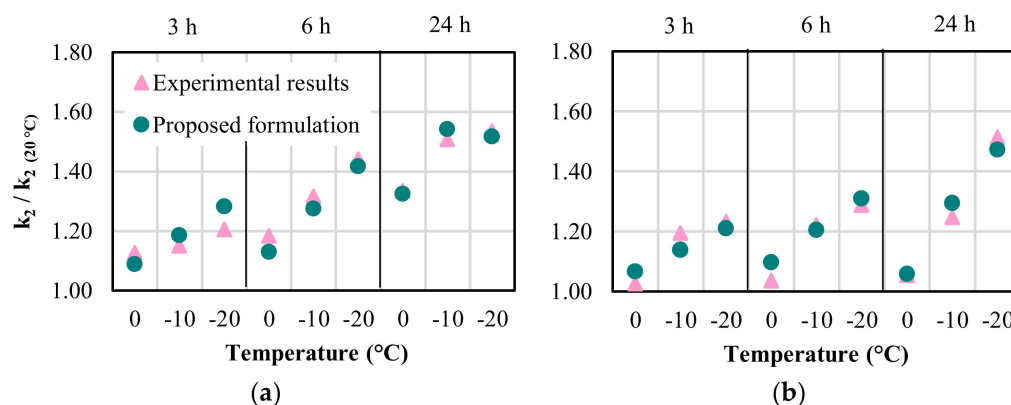
Figure 22. Comparison of experimental amplifications in k_2 with the proposed formulation estimations for 0.5 Hz loading frequency at (**a**) 100% and (**b**) 134% shear strains.

6. Conclusions

In this study, a large-size LRB exposed to low temperatures (0, -10, and -20 °C) for several exposure times (3, 6, and 24 h) was tested under dynamic conditions. In the tests, displacement-controlled cyclic motions were applied with different shear strains (100 and 134% and loading frequencies (0.1 and 0.5 Hz). Based on the test results, amplifications in characteristic strength and post-yield stiffness of the tested LRB were investigated. In addition, new equations were proposed to estimate the amount of amplification in the mechanical properties of LRBs while evaluating the accuracy of the available equations in the literature. The following conclusions are drawn based on the results:

1. Mechanical properties of the LRB, namely, characteristic strength and post-yield stiffness, increase as the temperature decreases. However, characteristic strength is more sensitive to temperature change than post-yield stiffness. The amplification factors computed for the characteristic strength of the LRB are larger than those obtained for post-yield stiffness and can reach up to two.
2. Amplifications in both characteristic strength and post-elastic stiffness are highly sensitive to time of exposure to low temperatures. Longer exposure times resulted in larger amplifications in both properties of the LRB.
3. The effect of loading velocity is more pronounced for post-yield stiffness. The amplifications computed for post-yield stiffness are larger in tests with 0.5 Hz frequency compared to those of 0.1 Hz. There is a tendency for amplifications of post-yield stiffness to increase with increasing loading velocity.
4. The existing equations proposed to predict the amplifications in the characteristic strength and post-yield stiffness of LRBs at low temperatures are in lack of considering the effects of exposure time, loading frequency, and the amplitude of the motion. The empirical equations proposed in this study have considered all these effects, and their estimations are found to be in good agreement with experimental data.

In order to refrain from overgeneralization, it should be noted that the presented results are specific to the tested LRB and the loading protocol (shear strains, loading frequencies, low temperatures, and exposure times) used in the research.

Data Availability Statement: All data, models, or code that support the findings of this study are available from the corresponding author upon reasonable request.

Conflicts of Interest: The authors declare no conflict of interest.

References

1. Skinner, R.I.; Robinson, W.H.; McVerry, G.H. *An Introduction to Seismic Isolation*; Wiley: New York, NY, USA, 1993.
2. Naeim, F.; Kelly, J.M. *Design of Seismic Isolated Structures: From Theory to Practice*; Wiley: New York, NY, USA, 1999.
3. Pan, P.; Zamfirescu, D.; Nakashima, M.; Nakayasu, N.; Kashiwa, H. Base-isolation design practice in Japan: Introduction to the post-kobe approach. *J. Earthq. Eng.* **2005**, *9*, 147–171. [CrossRef]
4. Roeder, C.W.; Stanton, J.F.; Feller, T. Low-temperature performance of elastomeric bearings. *J. Cold Reg. Eng.* **1990**, *4*, 113–132. [CrossRef]
5. Yakut, A.; Yura, J.A. Parameters influencing performance of elastomeric bearings at low temperatures. *J. Struct. Eng.* **2002**, *128*, 986–994. [CrossRef]
6. Yakut, A.; Yura, J.A. Evaluation of low-temperature test methods for elastomeric bridge bearings. *J. Bridge Eng.* **2002**, *7*, 50–56. [CrossRef]
7. Fuller, K.N.G.; Gough, J.; Thomas, A.G. The effect of low-temperature crystallization on the mechanical behaviour of rubber. *J. Polym. Sci. Part B Polym. Phys.* **2004**, *42*, 2181–2190. [CrossRef]
8. Pınarbası, S.; Akyuz, U. Seismic isolation and elastomeric bearing tests. *IMO Tech. J.* **2005**, *237*, 3581–3598.
9. Pınarbasi, S.; Akyuz, U.; Ozdemir, G. An experimental study on low temperature behavior of elastomeric bridge bearing. In Proceedings of the 10th World Conference on Seismic Isolation, Energy Dissipation and Active Vibrations Control of Structures, Istanbul, Turkey, 28–31 May 2007.
10. Cardone, D.; Gesualdi, G. Experimental evaluation of the mechanical behavior of elastomeric materials for seismic applications at different air temperatures. *Int. J. Mech. Sci.* **2012**, *64*, 127–143. [CrossRef]
11. Ozturk, H. Effects of Lead Core Heating on the Response of Isolated-Base and Fixed-Base Regular and Irregular Reinforced Concrete Structures. *Buildings* **2022**, *12*, 1087. [CrossRef]
12. Fujii, K.; Mogi, Y.; Noguchi, T. Predicting maximum and cumulative response of a base-isolated building using pushover analyses. *Buildings* **2020**, *10*, 91. [CrossRef]
13. Robinson, W.H. Lead-rubber hysteretic bearings suitable for protecting structures during earthquakes. *Earthq. Eng. Struct. Dyn.* **1982**, *10*, 593–604. [CrossRef]
14. Hasegawa, O.; Shimoda, I.; Ikenaga, M. Characteristic of lead rubber bearing by temperature. In *Summaries of Technical Papers of Annual Meeting Architectural Institute of Japan, B-2, Structures II, Structural Dynamics Nuclear Power Plants*; Architectural Institute of Japan: Tokyo, Japan, 1997; pp. 511–512. (In Japanese)
15. Constantinou, M.C.; Whittaker, A.S.; Kalpakidis, Y.; Fenz, D.M.; Warn, G.P. Performance of seismic isolation hardware under service and seismic loading. In *Technical Report, MCEER-07-0012, Multidisciplinary Center for Earthquake Engineering Research*; State University of New York: Buffalo, NY, USA, 2007.
16. Li, J.; Ye, K.; Jiang, Y.C. Thermal effect on the mechanical behavior of lead-rubber bearing. *J. Huazhong Univ. Sci. Technol. Med. Sci.* **2009**, *138*, 867–876.
17. Cho, C.B.; Khawk, I.J.; Kim, Y.J. An experimental study for the shear property and the temperature dependency of seismic isolation bearings. *J. Earthq. Eng. Soc. Korea* **2008**, *12*, 67–77.
18. Park, J.Y.; Jang, K.S.; Lee, H.P.; Lee, Y.H.; Kim, H. Experimental study on the temperature dependency of full-scale low hardness lead rubber bearing. *J. Comput. Struct. Eng. Inst. Korea* **2012**, *25*, 533–540. [CrossRef]
19. Mendez-Galindo, C.; Moor, G.; Rassy, S. Lead rubber bearings for seismic isolation of structures in cold climates-new developments. In Proceedings of the 39th IABSE Symposium–Engineering the Future, Vancouver, BC, Canada, 21–23 September 2017; pp. 54–63.
20. Zhang, R.; Li, A. Experimental study on temperature dependence of mechanical properties of scaled high-performance rubber bearings. *Compos. Part B Eng.* **2020**, *190*, 107932. [CrossRef]
21. Cavdar, E.; Ozdemir, G.; Karuk, V. Modification in response of a bridge seismically isolated with lead rubber bearings exposed to low temperature. *IMO Tech. J.* **2022**, *33*, 12553–12576.
22. *EN 15129:2018*; Anti-Seismic Devices. European Committee for Standardization (CEN): Brussel, Belgium, 2018.
23. Kalpakidis, I.; Constantinou, M.C.; Whittaker, A.S. Modeling strength degradation in lead-rubber bearings under earthquake shaking. *Earthq. Eng. Struct. Dyn.* **2010**, *39*, 1533–1549. [CrossRef]
24. Cramer, N.L. A representation for the adaptive generation of simple sequential programs. In *Proceedings of the First International Conference on Genetic Algorithms and Their Applications*; Grefenstette, J.J., Ed.; Psychology Press: London, UK, 1985; pp. 183–187.
25. Koza, J.R. *Genetic Programming: On the Programming of Computers by Means of Natural Selection*; MIT Press: Cambridge, MA, USA, 1992.
26. Ferreira, C. *Gene Expression Programming, Mathematical Modeling by an Artificial Intelligence (Studies in Computational Intelligence)*; Springer: Secaucus, NJ, USA, 2002.

27. Soh, C.K.; Yang, Y. Genetic programming-based approach for structural optimization. *J. Comput. Civ. Eng.* **2000**, *14*, 31–37. [CrossRef]

28. Ashour, A.F.; Alvarez, L.F.; Toropov, V.V. Empirical modelling of shear strength of RC deep beams by genetic programming. *Comput. Struct.* **2003**, *81*, 331–338. [CrossRef]

29. Gandomi, A.H.; Alavi, A.H.; Sahab, M.G.; Arjmandi, P. Formulation of elastic modulus of concrete using linear genetic programming. *J. Mech. Sci. Technol.* **2010**, *24*, 1273–1278. [CrossRef]

30. Chen, H.M.; Kao, W.K.; Tsai, H.C. Genetic programming for predicting a seismic abilities of school buildings. *Eng. Appl. Artif. Intell.* **2012**, *25*, 1103–1113. [CrossRef]

31. Caglar, N.; Demir, A.; Ozturk, H.; Akkaya, A. A simple formulation for effective flexural stiffness of circular reinforced concrete columns. *Eng. Appl. Artif. Intell.* **2015**, *38*, 79–87. [CrossRef]

32. GeneXproTools. Gene Expression Programming Tools. Gepsoft Limited, 2000, 73 Elmtree Drive Bristol BS 13 8NA United Kingdom. Available online: http://www.gepsoft.com (accessed on 8 November 2022).